Research Article

# Molecular Insights into Hybrid CH$_4$ Physisorption-Hydrate Formation in Spiral Halloysite Nanotubes: Implications for Energy Storage

Fengyi Mi, Zhongjin He,* Jiangtao Pang, Othonas A. Moultos, Thijs J. H. Vlugt, and Fulong Ning

Cite This: *ACS Appl. Mater. Interfaces* 2024, 16, 67587−67596
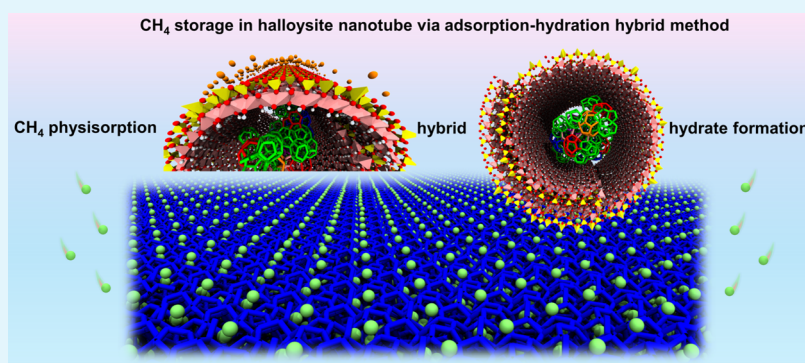
Read Online

ACCESS | Metrics & More | Article Recommendations | SI Supporting Information



CH$_4$ storage in halloysite nanotube via adsorption-hydration hybrid method

CH$_4$ physisorption — hybrid — hydrate formation

**ABSTRACT:** A microscopic insight into hybrid CH$_4$ physisorption-hydrate formation in halloysite nanotubes (HNTs) is vital for understanding the solidification storage of natural gas in the HNTs and developing energy storage technology. Herein, large-scale microsecond classical molecular dynamics simulations are conducted to investigate CH$_4$ storage in the HNTs via the adsorption-hydration hybrid (AHH) method to reveal the effect of gas−water ratio. The simulation results indicate that the HNTs are excellent nanomaterials for CH$_4$ storage via the adsorption-hydration hybrid method. The CH$_4$ physisorption and hydrate formation inside and outside of the HNTs are profoundly influenced by the surface properties of the HNTs and the kinetic characteristics of CH$_4$/H$_2$O molecules. The outer surfaces of the HNTs exhibit relative hydrophobicity and adsorb CH$_4$ molecules to form nanobubbles. Moreover, CH$_4$ molecules adsorbed on the outer surface are tightly trapped between the hydrate solids and the outer surface, inhibiting their kinetic behavior and favoring CH$_4$ storage via physisorption. The inner surface of the HNTs exhibits extreme hydrophilicity and strongly adsorbs H$_2$O molecules; thus, CH$_4$ hydrate can form inside of the HNTs. It is more difficult for CH$_4$ and H$_2$O molecules inside of the HNTs to convert into hydrates than for those outside of the HNTs. A moderate gas−water ratio is advantageous for CH$_4$ physisorption and hydrate formation, whereas excessively high or low gas−water ratios are unfavorable for efficient CH$_4$ storage. These insights can help to develop an efficient CH$_4$ solidification storage technology.

**KEYWORDS:** methane storage, halloysite nanotube, molecular dynamics simulation, physisorption, hydrate formation, methane hydrate, surface property

## INTRODUCTION

Challenges loom large on the global stage with energy shortages and climate deterioration, as we grapple with the continuous surge in energy consumption.[1] The imminent exhaustion of traditional fossil fuel reserves and the escalating greenhouse effect underscore the urgency of our quest to explore and advance clean energy.[1] Natural gas (mainly CH$_4$) stands out with its abundant reserves and low CO$_2$ emissions, positioning it as a relatively clean fuel with a great potential to meet all of the energy demands of modern society in the coming decades.[2] Its significance in our daily lives is already irreplaceable and continues to grow. However, the limitation of natural gas is that the mass density of CH$_4$ is low, which increases the cost of natural gas storage and transportation.

Pipeline natural gas (PNG), compressed natural gas (CNG), liquefied natural gas (LNG), and other technologies all face safety risks and low gas storage capacity. An innovative method of solidifying natural gas (SNG) has been proposed through the utilization of clathrate hydrates.[3−5] Clathrate hydrates are ice-like nonstoichiometric crystalline solids in which gas molecules are encapsulated in the hydrogen-bonds framework
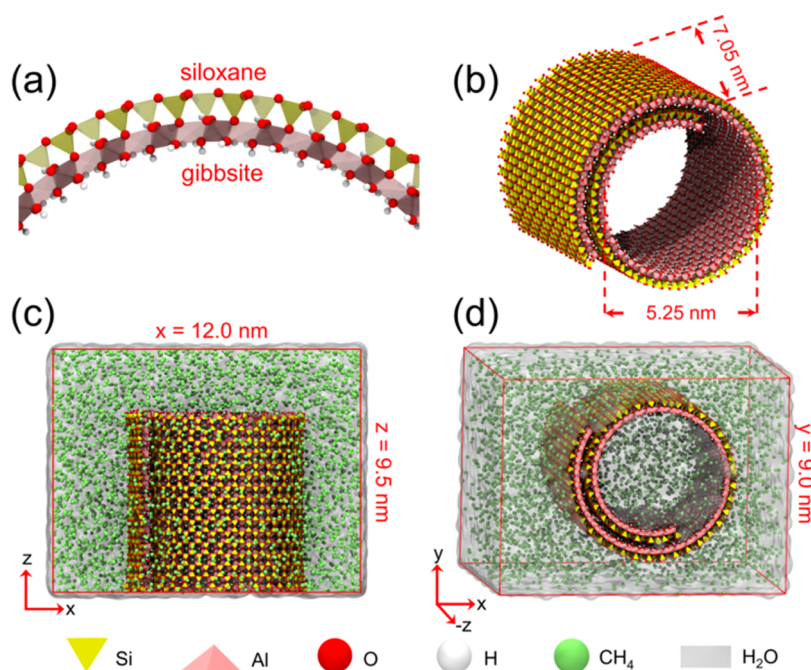
67587
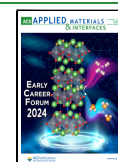
**Figure 1.** (a, b) Schematic diagram of the HNTs and configuration diagram (c, d) of the final simulation model.

of water molecules.[6] One of the most attractive aspects of clathrate hydrates is that the 1 m[3] of CH$_4$ hydrate contains up to 160 m[3] of CH$_4$ gas.[6] Hydrates are formed under comparatively mild conditions compared to the compression and liquefaction of natural gas. Nonetheless, the long hydrate induction time and low water-hydrate conversion ratio become roadblocks to the development of this method.[5]

Significant efforts have been dedicated to accelerating hydrate formation and enhancing conversion ratio, including the use of mechanical reinforcements,[7,8] chemical additives,[9−11] and porous materials.[12−15] In particular, porous materials stand out due to their large specific surface area and favorable surface physicochemical properties, which promote CH$_4$ hydrate formation and increase conversion ratio.[16−21] Various experimental studies have employed carbon nanotubes,[22−24] silicas,[25−27] activated carbon,[28−31] metal−organic frameworks,[32−35] zeolites,[36−39] and other materials[40−43] as the hydrate promoters to augment CH$_4$ storage. Recently, the adsorption-hydration hybrid (AHH) method has been proposed as a more efficient gas storage technology, i.e., CH$_4$ is solidified and stored through the hybrid of adsorption and hydrate formation. This innovative technology leverages the synergistic effect of CH$_4$ physisorption and CH$_4$ hydrate formation in porous materials, greatly enhancing CH$_4$ storage capacity under mild conditions.[44−46] Despite these advancements, the microscopic mechanism of CH$_4$ physisorption and hydrate formation in porous materials remain elusive. Molecular dynamics (MD) simulation is a valuable tool for studying the microscopic behavior of clathrate hydrates.[47,48] Microsecond MD simulations have been performed to study CH$_4$ hydrate formation in the mesoporous metal−organic framework MIL-101, and the results indicated that CH$_4$ hydrate was preferentially formed in the outer space of the MIL-101 cavity rather than inside the cavity.[49,50] The MD results of Wang et al. revealed the relationship between CH$_4$ physical adsorption and CH$_4$ hydrate growth in the hydrophobic metal−organic framework ZIF-8.[51] Based on MD simulations, the results of Duan et al. showed that the larger

gas−liquid ratio can accelerate the transportation of ZIF-8 intergranular CH$_4$ and H$_2$O at early stage to promote hydrate nucleation and growth.[52] Li and co-workers found that when the water content was sufficient, the gas adsorption performance of ZIF-8 solid particles could significantly accelerate the hydrate nucleation, exhibiting the adsorption-hydration synergy.[53] Wu et al. revealed through MD simulation that the substrate surface hydrophilicity significantly affects hydrate formation and thus changes the CH$_4$ storage capacity.[54]

While MOFs and activated carbon possess large specific surface areas that promote gas adsorption, their monotonous surface property may limit water adsorption and not good for hydrate formation in confined spaces. Moreover, MOFs and activated carbon are expensive to synthesize and not as readily available. In contrast, halloysite nanotubes (HNTs) are one kind of nanomaterial available in thousands of tons at low prices.[55] It is a nontoxicity, biocompatible, and readily available alumosilicate and has attracted interest as an efficient container for storing CH$_4$.[55] The surface properties of the hollow tubular shape nanotubes closely resemble those of kaolinite, with the outer surface composed of hydrophobic siloxane and the inner lumen surface composed of hydrophilic gibbsite (Figure 1a,b).[56] This unique Janus surface of HNTs could facilitate both water adsorption (for hydrate formation) and CH$_4$ physisorption. The unique shape and surface properties of halloysite nanotubes are expected to serve as efficient containers for CH$_4$ using the adsorption-hydration hybrid method. The experimental results of Em et al. show that the HNTs are well suited for the requirements of gas storage materials and the halloysite-bound water is almost fully transformed into hydrate in pores smaller than 10 nm.[57] The experiments by Stoporev and colleagues found that the HNTs promote hydrate nucleation by reducing the supercooling of the formed hydrate.[58] The physisorption process of CH$_4$ molecules in HNTs is unclear, and the microscopic mechanism of CH$_4$ hydrate formation in HNTs remains mysterious.

In this study, large-scale microsecond MD simulations are conducted to investigate CH$_4$ storage in spiral HNTs via the
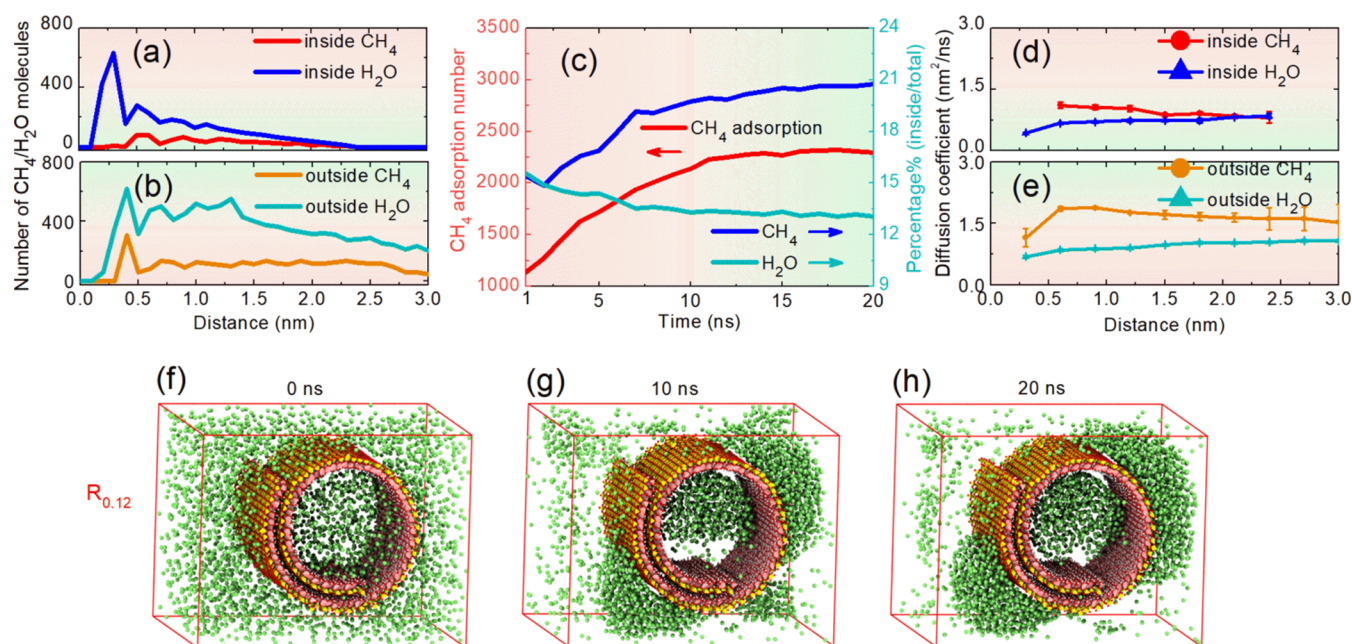
**Figure 2.** Number of (a, b) $CH_4$ and $H_2O$ molecules and (d, e) their diffusion coefficient ($K_{DC}$) at various radial distances from the inner and outer surfaces during the last 5 ns of 20 ns adsorption simulation for the $R_{0.12}$ simulation system. Each $K_{DC}$ is calculated within the range 0.3 nm. Evolution of the number of (c) $CH_4$ molecules adsorbed on the outer surface, and the dark blue (sky blue) curves represent the percentage of $CH_4$ molecules ($H_2O$ molecules) inside of the HNTs relative to the total number of $CH_4$ molecules ($H_2O$ molecules) in the system. The adsorption processes of $CH_4$ molecules inside and outside the HNTs (f−h) in the $R_{0.12}$ simulation system. Green balls represent $CH_4$ molecules.

adsorption-hydration hybrid method (Figure 1c,d). The hybrid effect of $CH_4$ physisorption and $CH_4$ hydrate formation in the HNTs is revealed. The effect of the gas−water ratio on the $CH_4$ storage efficiency in the HNTs is clarified. This molecular insight can help to develop efficient and sustainable natural gas storage technologies. This preliminary study of the microscopic mechanism of $CH_4$ physisorption and $CH_4$ hydrate formation in the HNTs may catalyze further innovative research, particularly with regard to their significance in energy gas solidification storage and other hydrate-based technologies.

## ■ RESULTS AND DISCUSSION

**$CH_4$ Physisorption on the Inner and Outer Surfaces of the HNTs.** The properties of the inner and outer surfaces of the HNTs significantly affect the physisorption behavior of the $CH_4/H_2O$ molecules. During the adsorption process, phase separation occurs shortly after the homogeneous $CH_4$ solution (Videos S1−S3). Outside of the HNTs, a large number of $CH_4$ molecules adsorb on the outer surface, forming semiellipsoidal $CH_4$ nanobubbles. Simultaneously, an ellipsoidal $CH_4$ nanobubble is observed inside the HNTs (Figures 2f−h and S2a−f). The inner and outer surfaces of the HNTs exhibit different affinities for $CH_4$ and $H_2O$ molecules. The numbers of $CH_4/H_2O$ molecules at various distances from the inner and outer surfaces are shown in Figures 2a,b, S3a−l, and S4a−d. Inside the HNTs, $H_2O$ molecules show a noticeable wave peak in the range of 0−0.4 nm. $CH_4$ molecules do not exhibit a comparable wave peak (Figures 2a and S4a,c). This phenomenon indicates that the inner surface of the HNTs strongly adsorbs $H_2O$ molecules and repels $CH_4$ molecules, which is attributed to the fact that the hydrophilic gibbsite surface can form hydrogen bonds with $H_2O$ molecules. Outside of the HNTs, both $CH_4$ and $H_2O$ molecules show an obvious wave peak in the range of 0−0.5 nm, indicating the relatively hydrophobic outer surface can adsorb $CH_4$ and $H_2O$

molecules. The sharp peak at 0.3−0.5 nm corresponds to the adsorption of $CH_4$ molecules onto the siloxane surface of the HNTs (Figures 2b and S4b,d). The observed affinities of siloxane surface for $CH_4$ molecules align with the properties of kaolinite surfaces reported in previous MD studies.[59] Furthermore, due to the irregular shape of the nanobubbles adsorbed on the outer surface (Figures 2h and S2c,f), the radial distribution of $CH_4$ molecules does not immediately decline, reflecting the broader spatial distribution of $CH_4$ molecules around the HNTs. The adsorption of $CH_4$ molecules on the outer surface is crucial to the storage of the energy gas $CH_4$. The number of $CH_4$ molecules adsorbed on the outer surface initially rises rapidly, eventually reaching a plateau value (Figures 2c and S5a,b). At the end of the 20 ns adsorption simulation, approximately 2250 $CH_4$ molecules adsorb on the outer surface for the $R_{0.12}$ simulation system (Figure 2c).

The kinetic characteristics of $CH_4/H_2O$ molecules also affect the physisorption behavior of $CH_4/H_2O$ molecules. A selective diffusion pattern is observed, with a few $H_2O$ molecules migrating from the inside to the outside of the HNTs, while a small number of $CH_4$ molecules diffuse in the opposite direction (Figures 2c and S6a−c). During the first 1−2 ns, the mass transfer of $CH_4$ molecules is not yet stable. The initial slight decrease in the percentage of $CH_4$ molecules inside the HNTs is related to the dynamic process of $CH_4$ nanobubble formation outside of HNTs (Figure 2c). The diffusion coefficients ($K_{DC}$) of $CH_4/H_2O$ molecules at various distances from the inner and outer surfaces in the adsorption simulations are analyzed, and the results are shown in Figures 2d,e and S7a−d. Inside the HNTs, $CH_4$ molecules closer to the inner surface exhibit higher $K_{DC}$ values, suggesting a tendency for less stable adsorption, while $H_2O$ molecules closer to the inner surface have lower $K_{DC}$ values, indicative of more stable adsorption (Figures 2d and S7a,c). The diffusion patterns of $CH_4/H_2O$ molecules outside of the HNTs mirror
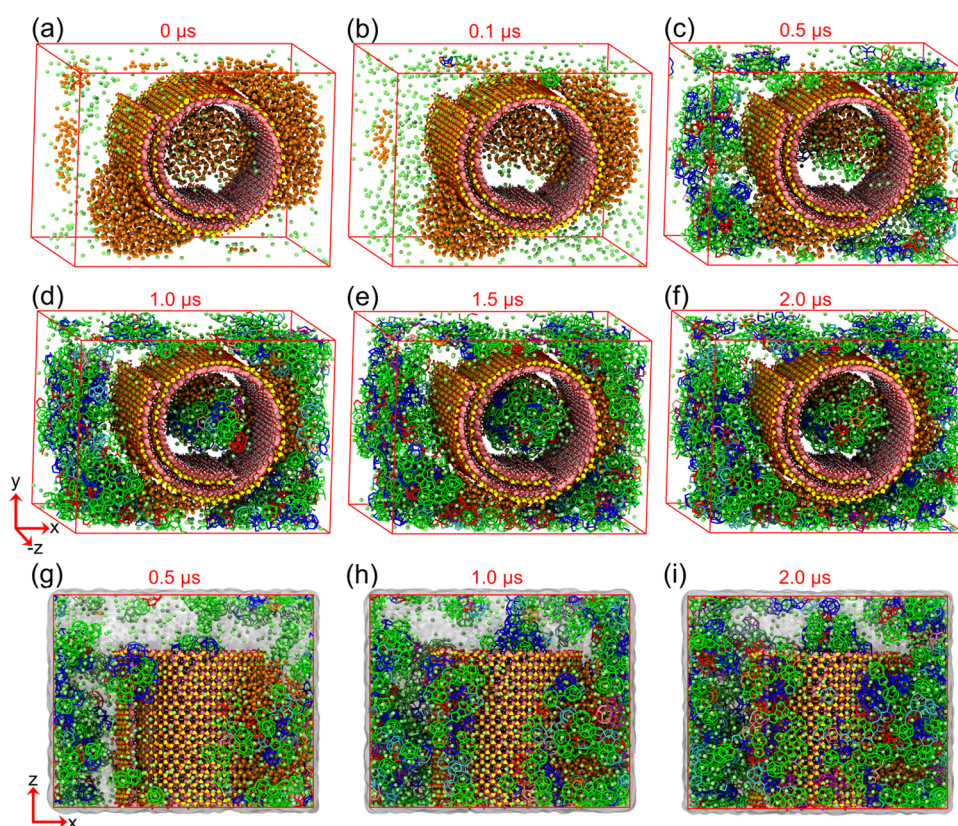
**Figure 3.** Formation processes of $CH_4$ hydrate inside and outside of the HNTs for the (a–i) $R_{0.12}$ simulation system. The HNTs are displayed as polyhedral, i.e., yellow (Si atom), and pink (Al atom). Orange and green balls represent $CH_4$ molecules in the nanobubble and solution, respectively. Hydrate cages are shown as sticks in various colors (green for $5^{12}$, blue for $5^{12}6^2$, red for $5^{12}6^3$, orange for $5^{12}6^4$, cyan for $4^1 5^{10}6^2$, purple for $4^1 5^{10}6^3$ and pink for $4^1 5^{10}6^4$).

those inside of the HNTs (Figures 2e and S7b,d). The diffusion abilities of $CH_4/H_2O$ molecules outside the HNTs are slightly larger than those inside the HNTs (Figures 2d,e and S7a–d). These observed properties of the inner and outer surfaces of the HNTs and kinetic characteristics of $CH_4/H_2O$ molecules inevitably play crucial roles in subsequent hydrate formation and distribution.

**Formation Kinetics of $CH_4$ Hydrate Inside and Outside of the HNT.** The formation kinetics of $CH_4$ hydrate inside and outside of the HNTs are profoundly influenced by the surface properties of the HNTs and the kinetic characteristics of $CH_4/H_2O$ molecules. $CH_4$ and $H_2O$ molecules outside of the HNTs are more easily converted into hydrates than those inside the HNTs. After the adsorption simulation, a large number of $CH_4$ molecules congregate to form nanobubbles inside and outside of the HNTs (Figures 3a, S8a, and S9a). These sizable $CH_4$ nanobubbles hinder the rapid nucleation of $CH_4$ hydrates during subsequent hydrate-formation simulations. In the early stages of the simulation, both inner and outer nanobubbles undergo a reduction in size (Figures 3b–e, S8b–e, and S9b–e). This reduction indicates a continuous transfer of $CH_4$ molecules from the nanobubbles to the solution, thereby augmenting the $CH_4$ concentration in the solution and facilitating hydrate nucleation (Figure S10). As the simulation progresses, several hydrate cages emerge inside and outside of the HNTs, gradually coalescing into hydrate clusters (Figures 3a–i, S8a–i, and S9a–i). A large number of $CH_4/H_2O$ molecules in solution transition into hydrates, and the conversion ratio of $CH_4/H_2O$ molecules inside and outside of the HNTs steadily rises (Figures 4a,b, S11a,b, and S12a,b).

Conversion ratio is defined as the ratio of the number of $CH_4/H_2O$ molecules in hydrate to their total number. Subsequently, these hydrate clusters develop into sizable hydrate solids both inside and outside of the HNTs, with numerous $CH_4/H_2O$ molecules forming hydrate cages (Figures S11c,d, S12c,d, and S13a,b). $CH_4$ mole fraction in water ($x_{CH_4}$) and $CH_4$ in the nanobubbles ($N_{CH4}$) inside and outside of the HNTs are analyzed in Figure 4c,d. In the $R_{0.12}$ simulation system, it is observed that the $CH_4$ nanobubbles inside the HNTs gradually become small in size, with $x_{CH_4}$ and $N_{CH4}$ values reaching 0.07 and 340, respectively (Figure 4c). The conversion ratio of $H_2O$ molecules inside of the HNTs increases rapidly, whereas the conversion ratio of $CH_4$ molecules shows a relatively slower increase (Figure 4a). At the end of the simulation, the conversion ratios of $CH_4/H_2O$ molecules inside of the HNTs reach approximately 18 and 33%, respectively (Figure 4a). These findings suggest that there are still a large number of $CH_4$ and $H_2O$ molecules that have yet to undergo hydrate conversion. Similarly, the $CH_4$ nanobubbles adsorbed on the outer surface diminish in size, allowing more $CH_4$ molecules to diffuse into the solution and form $CH_4$ hydrates with $H_2O$ molecules. At the end of the simulation, the $x_{CH_4}$ and $N_{CH4}$ values reach 0.087 and 720, respectively (Figure 4d). Moreover, the conversion ratios of $CH_4/H_2O$ molecules outside of the HNTs amount to approximately 28 and 41%, respectively, surpassing those observed inside the HNTs (Figure 4b). This disparity can be attributed to the strong binding of $H_2O$ molecules to the inner gibbsite surface of the HNTs (Figure S14a–c). Similar trends are observed from the
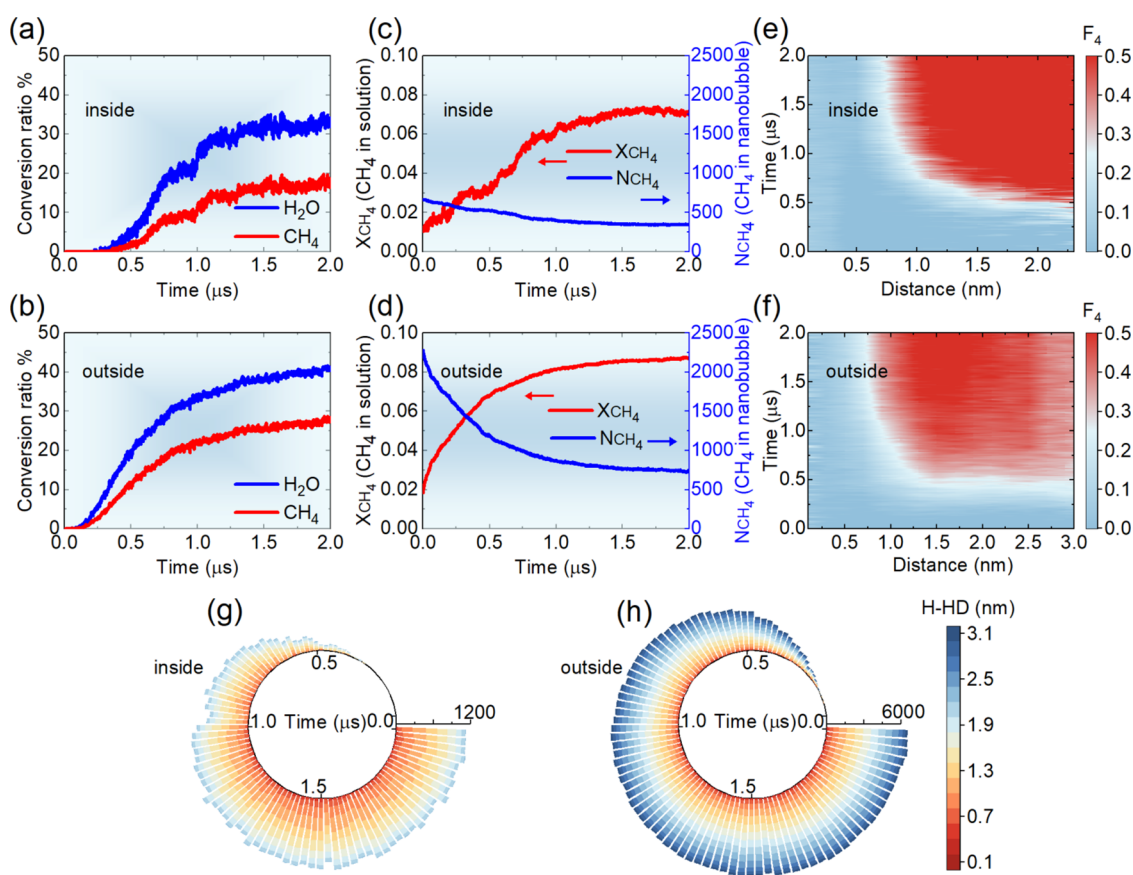
**Figure 4.** Evolution of (a, b) the conversion ratio of $CH_4/H_2O$ molecules, and (c, d) $CH_4$ mole fraction in water $x_{CH_4}$ and $CH_4$ in the nanobubbles $N_{CH4}$ inside and outside of the HNTs for the $R_{0.12}$ simulation system. Conversion ratio is defined as the number of $CH_4/H_2O$ ions in hydrate divided by their total number. Evolution of (e, f) the $F_4$ order parameter and (g, h) the number of $H_2O$ molecules in the hydrate as a function of the radial distance from the inner and outer surfaces of the HNTs (H-HD) for the $R_{0.12}$ simulation system.

$R_{0.148}$ and $R_{0.08}$ systems (Figures S15a−c and S16a−c). During the hydrate formation process, the mass transfer of $CH_4/H_2O$ molecules inside and outside of the HNTs exhibits no significant variation (Figure S17a−c).

The distribution of $CH_4$ hydrate inside and outside the HNTs exhibits intriguing properties. The $F_4$ order parameter serves as an effective discriminator for the water phase. The evolution of the $F_4$ value and the number of $H_2O$ molecules in hydrate at various radial distances from the inner and outer surfaces are illustrated in Figure 4e−h. In the early stages of the simulation, the $F_4$ value in the region 1.5−2.5 nm from the inner surface and 1.5−3.0 nm from the outer surface experiences a rapid increase (Figures 4e,f and S18a−f), indicating that $H_2O$ molecules situated far away from the inner and outer surfaces (i.e., closer to the gas−water interface) are first converted into hydrate. This observation suggests that $H_2O$ molecules near the gas−water interface in these regions are more easily converted into hydrate, as the interface provides an ideal environment for $CH_4$ hydrate nucleation and growth. In the HNTs, hydrates predominantly concentrate in the central region of the HNTs, as they cannot form near the inner gibbsite surface, owing to the presence of strongly bound water (Figures 4g and S19a−l). At the end of the simulation, the HNTs house primarily bound water, residual $CH_4$ nanobubbles and hydrate solids from outside to inside region in the $R_{0.12}$ simulation system (Figure 3f). Despite the fact that complete embedding of $CH_4$ hydrates inside of the HNTs is not being achieved, the composition of

bound water and hydrate solids still offers relatively stable and efficient $CH_4$ storage (Figure S20). In contrast, $CH_4$ hydrates outside of the HNTs are positioned relatively closer to the outer surface (Figures 4g,h and S19a−l). A large number of $CH_4$ and $H_2O$ molecules preferentially form hydrates in regions distanced from the outer surface, which gradually grow toward it (Figures 4h and S19a−l). This behavior stems from the $CH_4$ nanobubbles adsorbed on the outer surface, furnishing a sufficient gas source for hydrate formation. Consequently, $CH_4$ hydrate solids outside of the HNTs grow toward the $CH_4$ nanobubbles, aligning with the observations from previous MD studies. It is noteworthy that at the end of the simulation, although the near-external surface region lacks a significant number of $CH_4$ hydrate solids, the $CH_4$ nanobubbles adsorbed on the outer surface are encapsulated between the $CH_4$ hydrate solids and the HNTs (Figure 3f,i). Not only that, but the $CH_4$ nanobubbles exhibit an extremely small and flat shape in the $R_{0.12}$ simulation system (Figure 3f,i). Additionally, in the later stage of the simulation, the diffusion abilities of $CH_4$ molecules adsorbed on the outer siloxane surface sharply decrease (Figure S21a−l), realizing the strong physisorption on the outer surface of the HNTs to enhance $CH_4$ storage.

**Effect of Gas−Water Ratio on $CH_4$ Storage.** The gas/water ratio is a crucial parameter in hybrid $CH_4$ physisorption-hydrate formation. It is found that, in the physisorption processes, a moderate gas−water ratio is advantageous for $CH_4$ physisorption; excessively high or low gas−water ratios are
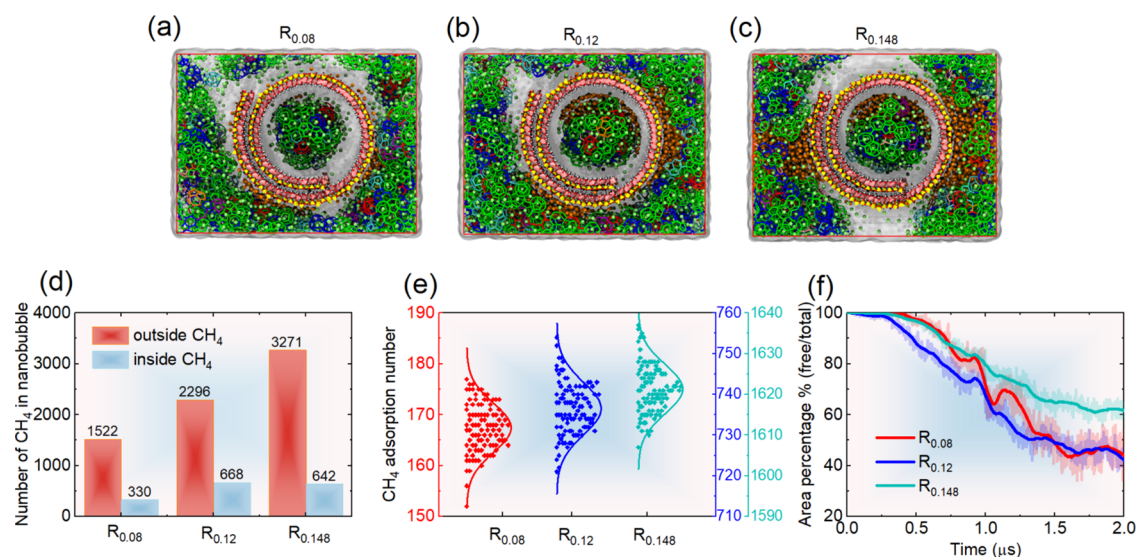
**Figure 5.** (a–c) Snapshots of $CH_4$ hydrate formed inside and outside of the HNTs at the end of 2 $\mu$s simulation in the $R_{0.08}$, $R_{0.12}$, and $R_{0.148}$ simulation systems. (d) Number of $CH_4$ in the nanobubbles $N_{CH4}$ at the end of 20 ns adsorption simulation and (e) the number of $CH_4$ adsorbed on the outer siloxane surface of the HNTs during the last 0.1 $\mu$s of the 2.0 $\mu$s hydrate-formation simulation for the three simulation systems. (f) Evolution of the area percentage of $CH_4$ nanobubbles for the three simulation systems. Area percentage is defined as the solvent accessible surface area of $CH_4$ nanobubbles that can contact with $H_2O$ molecules in solution (nonhydrate) divided by the total solvent accessible surface area.
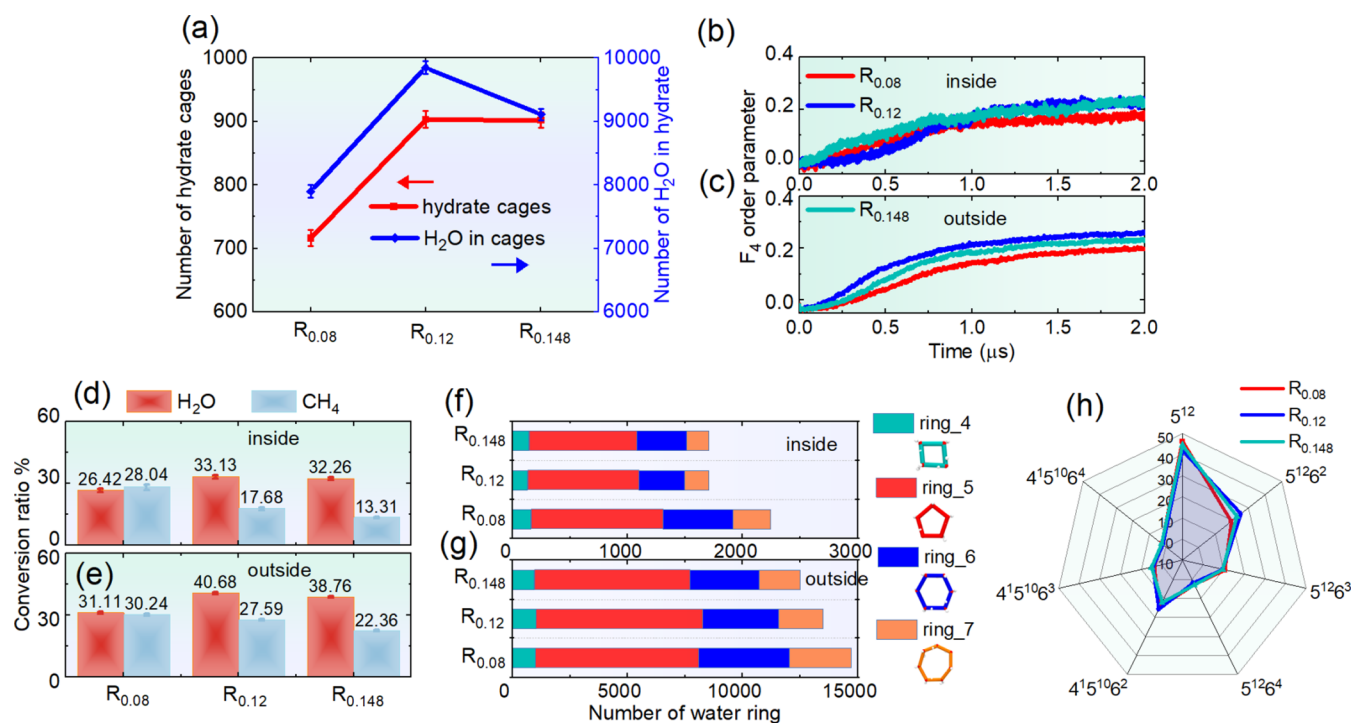


**Figure 6.** (a) Number of hydrate cages and $H_2O$ in hydrate cages in the three simulation systems. The evolution of (b, c) the $F_4$ order parameter, (d, e) the conversion ratio of $CH_4$/$H_2O$ molecules and (f, g) the number of water rings inside and outside of the HNTs in the three simulation systems. The (h) proportion of seven types of hydrate cages in the three simulation systems. The water ring, conversion ratio, and cage proportion are averaged over the last 0.1 $\mu$s of the 2.0-$\mu$s hydrate-formation simulation.

unfavorable for efficient energy storage. At the end of 20 ns adsorption simulation, the $N_{CH4}$ values outside of the HNTs in the $R_{0.08}$, $R_{0.12}$, and $R_{0.148}$ simulation systems amount to 1522, 2296, and 3271, respectively (Figure 5d). Higher gas/water ratios result in the formation of larger nanobubbles outside of the HNTs. The $N_{CH4}$ values inside of the HNTs are 330, 668, and 642 in the $R_{0.08}$, $R_{0.12}$, and $R_{0.148}$ simulation systems, respectively (Figure 5d). Remarkably, the $N_{CH4}$ values inside

the HNTs exhibit minimal disparity between the $R_{0.12}$ and $R_{0.148}$ simulation systems. This observation is attributed to the fixed volume of the HNTs, which accommodates a limited number of $CH_4$ molecules. Consequently, an excessively high gas−water ratio cannot significantly increase the number of $CH_4$ molecules inside the HNTs. The snapshots of three different gas−water ratios at the end of the 2-$\mu$s simulation are shown in Figure 5a−c. In the $R_{0.08}$ simulation system, the

majority of $CH_4$ molecules are converted into hydrates, and only a few $CH_4$ molecules adsorb on the outer surface of the HNTs (Figures 5a and S8f). Approximately 168 $CH_4$ molecules adsorb on the outer surface (Figure 5e). However, due to the low gas−water ratio, a large number of $H_2O$ molecules cannot be converted into hydrates. In the $R_{0.148}$ simulation system, numerous $CH_4$ molecules adsorb on the outer surface of the HNTs at 2 $\mu s$ (Figure 5c), with approximately 1620 $CH_4$ molecules adsorbed on the outer surface (Figure 5e). These $CH_4$ molecules are not entirely trapped by the $CH_4$ hydrate solid and the outer surface of the HNTs (Figures 5c and S9f). In contrast, in the $R_{0.12}$ simulation system, flat $CH_4$ molecules are trapped between the $CH_4$ hydrate solid and the outer surfaces of the HNTs (Figures 3f and 5b). Approximately 735 $CH_4$ molecules can be efficiently stored via physisorption (Figure 5e). To reveal the effect of the gas−water ratio on physisorption, the solvent accessible surface area (SASA) and area percentage of $CH_4$ molecules adsorbed on the outer surfaces of the HNTs are calculated (Figures 5f and S22a−c). Area percentage is defined as the solvent accessible surface area of $CH_4$ nanobubbles that can contact with $H_2O$ molecules in solution (nonhydrate) divided by the total solvent accessible surface area. This area percentage is mainly determined by the size and shape of the $CH_4$ nanobubbles, as well as the distribution of $CH_4$ hydrates around the $CH_4$ nanobubbles. The area percentage in the $R_{0.148}$ simulation system is the largest, followed by the $R_{0.08}$ simulation system, and finally the $R_{0.12}$ simulation system (Figures 5f and S22a−c). This observation indicates that at the end of the $R_{0.12}$ simulation, the $CH_4$ molecules adsorbed on the outer surface of the HNTs can be relatively tightly trapped by $CH_4$ hydrate solids and the outer surface of the HNTs, significantly inhibiting their kinetic behavior. This reduced kinetic behavior favors $CH_4$ storage via the adsorption-hydration hybrid method. Furthermore, at the end of the simulation, the area percentage of the $R_{0.08}$ simulation system is not markedly different from those in the $R_{0.12}$ simulation system (Figure 5f), which is attributable to the relatively small total SASA of the $R_{0.08}$ simulation system (Figure S22a).

In the hydrate formation process, a moderate gas/water ratio is also conducive to hydrate formation for $CH_4$ storage. At the end of the three simulations, the number of hydrate cages and $H_2O$ molecules in the hydrate cages are counted as shown in Figure 6a. It is found that the number of $H_2O$ molecules in the hydrate cage in the $R_{0.12}$ simulation system surpasses that in the $R_{0.08}$ and $R_{0.148}$ simulation systems (Figure 6a). Moreover, the number of hydrate cages in the $R_{0.12}$ simulation system is also slightly higher than that in the other two systems (Figures 6a and S23a−c). These findings suggest that the moderate gas−water ratio is more favorable for hydrate formation, consequently enhancing $CH_4$ storage via the adsorption-hydration hybrid method. The $F_4$ values inside of the HNTs reach 0.22, 0.22, and 0.17 for the $R_{0.148}$, $R_{0.12}$, and $R_{0.08}$ simulation systems, respectively (Figure 6b). The conversion ratios of $CH_4$ and $H_2O$ molecules in the $R_{0.12}$ simulation system are higher than those in the other two systems (Figure 6d). Similarly, the $F_4$ values outside of the HNTs reach 0.23, 0.26, and 0.20 for the $R_{0.148}$, $R_{0.12}$, and $R_{0.08}$ simulation systems, respectively (Figure 6c). The conversion ratios of $CH_4$ and $H_2O$ molecules in the $R_{0.12}$ simulation system are also higher than those in the $R_{0.08}$ and $R_{0.148}$ simulation systems (Figure 6e). These findings indicate that the conditions of the $R_{0.12}$ simulation system are more conducive to $CH_4$ hydrate

formation inside and outside of the HNTs (Figure S24), i.e., a moderate gas−water ratio is conducive to $CH_4$ storage via the adsorption-hydration hybrid method. On the other hand, the water ring and hydrate cage are crucial parameters for hydrate formation. Hydrate cages are composed of several water rings, and the number and type of water rings determine the structure of the hydrate cage. The number of water rings and the proportion of hydrate cages in the three simulation systems are illustrated in Figure 6f−h. It is observed that the number of five-membered rings inside and outside of the HNTs is the largest, followed by six-membered rings, with a small number of four- and seven-membered rings (Figures 6f,g and S25a−c). The number of six-membered rings in the $R_{0.08}$ simulation system is the largest (Figure 6f,g), which may be due to the difference in the number of $H_2O$ molecules in the three different simulation systems (Table S1). Additionally, it is found that $5^{12}$ cages and $5^{12}6^2$ cages show a higher proportion, followed by $4^1 5^{10} 6^2$ cages (Figures 6h and S26a−c). These small cages are the primary structures formed by $CH_4$ hydrate, which is also consistent with previous MD studies. The gas/water ratio exerts a slight influence on the cage proportion, primarily $5^{12}6^2$ cages. The formation processes of $CH_4$ hydrate inside and outside of the HNTs in the $R_{0.08}$, $R_{0.12}$ and $R_{0.148}$ simulation systems can be observed in Videos S4−S6, respectively.

## ■ CONCLUSIONS

Large-scale microsecond MD simulations are conducted to investigate $CH_4$ storage in the spiral halloysite nanotubes (HNTs) via the adsorption-hydration hybrid method to reveal the effects of the gas−water ratio. The simulation results indicate that the HNTs are excellent nanomaterials for $CH_4$ storage via the adsorption-hydration hybrid method. The $CH_4$ physisorption and hydrate formation inside and outside of the HNTs are profoundly influenced by the surface properties of the HNTs and the kinetic characteristics of $CH_4/H_2O$ molecules. The outer surfaces of the HNTs exhibit relative hydrophobicity and can adsorb $CH_4$ molecules. $CH_4$ molecules adsorbed on the outer surface of the HNTs are relatively tightly trapped between $CH_4$ hydrate solids and the outer surface of the HNTs, significantly inhibiting their kinetic behavior and favoring $CH_4$ storage via physisorption. The inner surface of the HNTs exhibits extreme hydrophilicity and can strongly adsorb $H_2O$ molecules; thus, $CH_4$ hydrate can form inside of the HNTs. It is more difficult for $CH_4$ and $H_2O$ molecules inside of the HNTs to convert into hydrates than those outside of the HNTs. $CH_4$ hydrate preferentially forms in regions away from the inner and outer surfaces of the HNTs and slowly grows toward these two surfaces. $CH_4$ hydrates outside of the HNTs are positioned relatively closer to the outer surface than those inside the HNTs. A moderate gas−water ratio is advantageous for $CH_4$ physisorption and $CH_4$ hydrate formation, whereas excessively high or low gas−water ratios are unfavorable for efficient $CH_4$ storage. These insights can help to develop an efficient and sustainable natural gas storage technology. This preliminary study into the microscopic mechanism of $CH_4$ physisorption and hydrate formation in the HNTs will catalyze further innovative research, particularly with regard to their significance in energy gas solidification storage and other hydrate-based technologies.

## METHODS

The halloysite nanotubes (HNTs) have a unique structure, featuring the hydrophobic siloxane on its outer surface and the hydrophilic gibbsite on its inner lumen surface. The unique structure of the HNTs is expected to efficiently store $CH_4$ via the adsorption-hydration hybrid method. We constructed a small HNTs model (Figure 1a), as larger models would dramatically increase the computational cost. This model draws inspiration from the work of Ferrante et al.[60] The inner lumen diameter of the HNTs is 10−100 nm and the length is 400−700 nm based on the general size distribution of natural HNTs.[56,60] However, such large inner diameter of the halloysite nanotubes requires the construction of an extremely large simulation model, which would greatly increase the computational cost. Therefore, the diameter of the inner lumen and length of the HNTs model were set to moderate values of 5.25 and 7.05 nm, respectively (Figure 1b). This HNT model was positioned in a simulation box with a size of $12.0 \times 9.0 \times 9.5$ nm$^3$ in the $xyz$ direction (Figure 1c,d). Subsequently, a homogeneous $CH_4$ solution with various gas−water ratios was added to the simulation box. Three simulation systems with different gas−water ratios, i.e., $R_{0.148}$, $R_{0.12}$, and $R_{0.08}$ were considered, where gas−water ratios in the homogeneous solution were set to 0.148, 0.12, and 0.08, respectively. To explore the physisorption processes of $CH_4$ molecules on the surface of the HNTs, a 20 ns adsorption simulation was performed under the isothermal−isobaric ($NPT$) ensemble. The temperature and pressure were 300 K and 10 MPa, respectively. The methods used to analyze the data can be found in the Supporting Information.

$CH_4$ and $H_2O$ molecules were represented by the OPLS-UA model[61] and TIP4P-ice model,[62] respectively. The HNT was represented using the CLAYFF force field,[63] which has been well-validated and widely used.[64,65] The detailed force field parameters for $H_2O$, $CH_4$, and HNT are shown in Table S2. A time step of 2.0 fs was used through the leapfrog algorithm. Periodic boundary conditions were imposed in all directions. All intermolecular nonbonded interaction was described by standard 12−6 Lennard−Jones (L−J) potentials, and the Lorentz−Berthelot combination rules were applied to calculate the interaction parameters between unlike LJ pairs. The particle-mesh Ewald (PME)[66] summation algorithm was used for the long-range electrostatic contributions within a Fourier space extending 12 Å. The cutoff distance of 10 Å was used for nonbonded interactions. The conditions of low temperature and high pressure in the simulations could accelerate hydrate formation and optimize computational efficiency.[67] An ultralong 2.0 μs production simulation was carried out under $NPT$ ensemble of 240 K and 10 MPa to explore hydrate formation in the system. During the 2.0 μs production simulation, the Nosé−Hoover thermostat[68] with a coupling time of 2 ps and the Parrinello−Rahman barostat[69] with a time constant equal to 4 ps were adopted to keep the temperature and pressure constant. All the molecular dynamics simulations were carried out using the GROMACS v.5.0.7.[70]

## ASSOCIATED CONTENT

### ⓈⒾ Supporting Information

The Supporting Information is available free of charge at https://pubs.acs.org/doi/10.1021/acsami.4c11288.

> Adsorption processes of $CH_4$ molecules inside and outside of the HNTs for the $R_{0.08}$ simulation system (Video S1) (AVI)
>
> Adsorption processes of $CH_4$ molecules inside and outside of the HNTs for the $R_{0.12}$ simulation system (Video S2) (AVI)
>
> Adsorption processes of $CH_4$ molecules inside and outside of the HNTs for the $R_{0.148}$ simulation system (Video S3) (AVI)
>
> Formation processes of $CH_4$ hydrates inside and outside of the HNTs for the $R_{0.08}$ simulation system (Video S4) (AVI)

> Formation processes of $CH_4$ hydrates inside and outside of the HNTs for the $R_{0.12}$ simulation system (Video S5) (AVI)
>
> Formation processes of $CH_4$ hydrates inside and outside of the HNTs for the $R_{0.148}$ simulation system (Video S6) (AVI)
>
> Additional methods; additional results and discussions; parameters for the simulation systems; schematic diagram of final simulation model; adsorption processes of $CH_4$; number of $CH_4/H_2O$ under different distances from surfaces; proportion of $CH_4/H_2O$ inside the halloysite; diffusion coefficient; formation processes of $CH_4$ hydrate; number density of $CH_4$; conversion ratio of $CH_4/H_2O$; $CH_4$ mole fraction, $CH_4$ in the nano-bubbles; $F_4$; solvent accessible surface area; hydrate cages; snapshot of water rings (PDF)

## AUTHOR INFORMATION

### Corresponding Author

**Zhongjin He** − *National Center for International Research on Deep Earth Drilling and Resource Development, Faculty of Engineering, China University of Geosciences, Wuhan, Hubei 430074, China;* ⓘ orcid.org/0000-0001-8850-3021; Email: hezhongjin@cug.edu.cn

### Authors

**Fengyi Mi** − *National Center for International Research on Deep Earth Drilling and Resource Development, Faculty of Engineering, China University of Geosciences, Wuhan, Hubei 430074, China; Engineering Thermodynamics, Process & Energy Department, Faculty of Mechanical Engineering, Delft University of Technology, Delft 2628CB, The Netherlands;* ⓘ orcid.org/0000-0002-1537-0683

**Jiangtao Pang** − *National Center for International Research on Deep Earth Drilling and Resource Development, Faculty of Engineering, China University of Geosciences, Wuhan, Hubei 430074, China;* ⓘ orcid.org/0000-0002-1882-9920

**Othonas A. Moultos** − *Engineering Thermodynamics, Process & Energy Department, Faculty of Mechanical Engineering, Delft University of Technology, Delft 2628CB, The Netherlands;* ⓘ orcid.org/0000-0001-7477-9684

**Thijs J. H. Vlugt** − *Engineering Thermodynamics, Process & Energy Department, Faculty of Mechanical Engineering, Delft University of Technology, Delft 2628CB, The Netherlands;* ⓘ orcid.org/0000-0003-3059-8712

**Fulong Ning** − *National Center for International Research on Deep Earth Drilling and Resource Development, Faculty of Engineering, China University of Geosciences, Wuhan, Hubei 430074, China;* ⓘ orcid.org/0000-0003-1236-586X

Complete contact information is available at:
https://pubs.acs.org/10.1021/acsami.4c11288

### Notes

The authors declare no competing financial interest.

## ACKNOWLEDGMENTS

## ■ REFERENCES

(1) Schneider, S. H. The greenhouse effect: science and policy. *Science* **1989**, *243* (4892), 771−781.

(2) Smil, V. *Natural Gas: Fuel for the 21st Century*; John Wiley & Sons, 2015.

(3) Koh, C. A. Towards a fundamental understanding of natural gas hydrates. *Chem. Soc. Rev.* **2002**, *31* (3), 157−167.

(4) Englezos, P.; Lee, J. D. Gas hydrates: A cleaner source of energy and opportunity for innovative technologies. *Korean J. Chem. Eng.* **2005**, *22* (5), 671−681.

(5) Veluswamy, H. P.; Kumar, A.; Seo, Y.; Lee, J. D.; Linga, P. A review of solidified natural gas (SNG) technology for gas storage via clathrate hydrates. *Appl. Energy* **2018**, *216*, 262−285.

(6) Sloan, E. D.; Koh, C. A. *Clathrate Hydrates of Natural Gases*; CRC Press, 2008.

(7) Zhang, G. D.; Shi, X. Y.; Liu, Z.; Wang, F. The synergy of spiral agitation and nano-promoters significantly enhances hydrate formation under mild conditions. *Chem. Eng. J.* **2022**, *450*, No. 138354.

(8) Hao, W. F.; Wang, J. Q.; Fan, S. S.; Hao, W. B. Study on methane hydration process in a semi-continuous stirred tank reactor. *Energy Convers. Manage.* **2007**, *48* (3), 954−960.

(9) Kumar, A.; Bhattacharjee, G.; Kulkarni, B. D.; Kumar, R. Role of Surfactants in Promoting Gas Hydrate Formation. *Ind. Eng. Chem. Res.* **2015**, *54* (49), 12217−12232.

(10) Liu, X. J.; Li, Y.; Chen, G. J.; Chen, D. Y.; Sun, B.; Yin, Z. Y. Coupling Amino Acid with THF for the Synergistic Promotion of $CO_2$ Hydrate Micro Kinetics: Implication for Hydrate-Based $CO_2$ Sequestration. *ACS Sustainable Chem. Eng.* **2023**, *11* (15), 6057−6069.

(11) Zhao, Y.; Yang, M.; Li, M.; Dong, H.; Ge, Y.; Li, Q.; Zhang, L.; Liu, Y.; Yang, L.; Song, Y.; Zhao, J. Magnetically Recyclable − $SO_3^-$-Coated Nanoparticles Promote Gas Storage via Forming Hydrates. *ACS Appl. Mater. Interfaces* **2022**, *14* (29), 33141−33150.

(12) Zhang, G. D.; Zhang, R. C.; Wang, F. Fast formation kinetics of methane hydrates loaded by silver nanoparticle coated activated carbon (Ag-NP@AC). *Chem. Eng. J.* **2021**, *417*, No. 129206.

(13) Casco, M. E.; Silvestre-Albero, J.; Ramirez-Cuesta, A. J.; Rey, F.; Jorda, J. L.; Bansode, A.; Urakawa, A.; Peral, I.; Martinez-Escandell, M.; Kaneko, K.; Rodríguez-Reinoso, F. Methane hydrate formation in confined nanospace can surpass nature. *Nat. Commun.* **2015**, *6* (1), No. 6432.

(14) Casco, M. E.; Rey, F.; Jorda, J. L.; Rudic, S.; Fauth, F.; Martinez-Escandell, M.; Rodriguez-Reinoso, F.; Ramos-Fernandez, E. V.; Silvestre-Albero, J. Paving the way for methane hydrate formation on metal-organic frameworks (MOFs). *Chem. Sci.* **2016**, *7* (6), 3658−3666.

(15) Wang, L.; Dou, M.; Wang, Y.; Xu, Y.; Li, Y.; Chen, Y.; Li, L. A Review of the Effect of Porous Media on Gas Hydrate Formation. *ACS Omega* **2022**, *7* (38), 33666−33679.

(16) Nguyen, N. N.; Nguyen, A. V. Hydrophobic Effect on Gas Hydrate Formation in the Presence of Additives. *Energ Fuels* **2017**, *31* (10), 10311−10323.

(17) Qin, Y.; Shang, L. Y.; Lv, Z. B.; He, J. Y.; Yang, X.; Zhang, Z. Methane hydrate formation in porous media: Overview and perspectives. *J. Energy Chem.* **2022**, *74*, 454−480.

(18) Both, A. K.; Gao, Y.; Zeng, X. C.; Cheung, C. L. Gas hydrates in confined space of nanoporous materials: new frontier in gas storage technology. *Nanoscale* **2021**, *13* (16), 7447−7470.

(19) Shi, C.; Wang, S.; Liu, H.; Zhang, L.; Yang, M.; Song, Y.; Zhao, J.; Ling, Z. Pyrolytic aerogels with tunable surface groups for efficient methane solidification storage via gas hydrates. *Fuel* **2023**, *331*, No. 125716.

(20) Nguyen, N. N.; Nguyen, A. V. "Nanoreactors" for Boosting Gas Hydrate Formation toward Energy Storage Applications. *ACS Nano* **2022**, *16* (8), 11504−11515.

(21) Zhang, Z.; Kusalik, P. G.; Liu, C.; Wu, N. Methane hydrate formation in slit-shaped pores: Impacts of surface hydrophilicity. *Energy* **2023**, *285*, No. 129414.

(22) Park, S. S.; Lee, S. B.; Kim, N. J. Effect of multi-walled carbon nanotubes on methane hydrate formation. *J. Ind. Eng. Chem.* **2010**, *16* (4), 551−555.

(23) Li, T. Y.; Liu, N.; Huang, J. L. Effects of carbon nanotube on methane hydrate formation by molecular dynamics simulation. *J. Mol. Liq.* **2022**, *368*, No. 120621.

(24) Zhao, W.; Wang, L.; Bai, J.; Francisco, J. S.; Zeng, X. C. Spontaneous formation of one-dimensional hydrogen gas hydrate in carbon nanotubes. *J. Am. Chem. Soc.* **2014**, *136* (30), 10661−10668.

(25) Casco, M. E.; Grätz, S.; Wallacher, D.; Grimm, N.; Többens, D. M.; Bilo, M.; Speil, N.; Fröba, M.; Borchardt, L. Influence of surface wettability on methane hydrate formation in hydrophilic and hydrophobic mesoporous silicas. *Chem. Eng. J.* **2021**, *405*, No. 126955.

(26) He, Z.; Mi, F.; Ning, F. Molecular insights into $CO_2$ hydrate formation in the presence of hydrophilic and hydrophobic solid surfaces. *Energy* **2021**, *234*, No. 121260.

(27) Prasad, P. S. R.; Sowjanya, Y.; Chari, V. D. Enhancement in Methane Storage Capacity in Gas Hydrates Formed in Hollow Silica. *J. Phys. Chem. C* **2014**, *118* (15), 7759−7764.

(28) Siangsai, A.; Rangsunvigit, P.; Kitiyanan, B.; Kulprathipanja, S.; Linga, P. Investigation on the roles of activated carbon particle sizes on methane hydrate formation and dissociation. *Chem. Eng. Sci.* **2015**, *126*, 383−389.

(29) Yan, L.; Chen, G.; Pang, W.; Liu, J. Experimental and modeling study on hydrate formation in wet activated carbon. *J. Phys. Chem. B* **2005**, *109* (12), 6025−6030.

(30) Govindaraj, V.; Mech, D.; Pandey, G.; Nagarajan, R.; Sangwai, J. S. Kinetics of methane hydrate formation in the presence of activated carbon and nano-silica suspensions in pure water. *J. Nat. Gas Sci. Eng.* **2015**, *26*, 810−818.

(31) Zhang, R. C.; Zhang, G. D.; Wang, F. Hydrate Formation Loaded by an Activated Carbon Bed in 3D-Printed Containers. *Energ Fuels* **2021**, *35* (19), 15675−15683.

(32) Denning, S.; Majid, A. A. A.; Lucero, J. M.; Crawford, J. M.; Carreon, M. A.; Koh, C. A. Methane Hydrate Growth Promoted by Microporous Zeolitic Imidazolate Frameworks ZIF-8 and ZIF-67 for Enhanced Methane Storage. *ACS Sustainable Chem. Eng.* **2021**, *9* (27), 9001−9010.

(33) Denning, S.; Majid, A. A.; Lucero, J. M.; Crawford, J. M.; Carreon, M. A.; Koh, C. A. Metal-Organic Framework HKUST-1 Promotes Methane Hydrate Formation for Improved Gas Storage Capacity. *ACS Appl. Mater. Interfaces* **2020**, *12* (47), 53510−53518.

(34) Cuadrado-Collados, C.; Mouchaham, G.; Daemen, L.; Cheng, Y.; Ramirez-Cuesta, A.; Aggarwal, H.; Missyul, A.; Eddaoudi, M.; Belmabkhout, Y.; Silvestre-Albero, J. Quest for an Optimal Methane Hydrate Formation in the Pores of Hydrolytically Stable Metal-Organic Frameworks. *J. Am. Chem. Soc.* **2020**, *142* (31), 13391−13397.

(35) Wang, P.; Teng, Y.; Zhu, J.; Bao, W.; Han, S.; Li, Y.; Zhao, Y.; Xie, H. Review on the synergistic effect between metal−organic frameworks and gas hydrates for $CH_4$ storage and $CO_2$ separation applications. *Renewable Sustainable Energy Rev.* **2022**, *167*, No. 112807.

(36) Zhao, Y. S.; Zhao, J. Z.; Liang, W. G.; Gao, Q.; Yang, D. Semi-clathrate hydrate process of methane in porous media-microporous materials of 5A-type zeolites. *Fuel* **2018**, *220*, 185−191.

(37) Andres-Garcia, E.; Dikhtiarenko, A.; Fauth, F.; Silvestre-Albero, J.; Ramos-Fernández, E. V.; Gascon, J.; Corma, A.; Kapteijn, F. Methane hydrates: Nucleation in microporous materials. *Chem. Eng. J.* **2019**, *360*, 569−576.

(38) Denning, S.; Majid, A. A. A.; Crawford, J. M.; Carreon, M. A.; Koh, C. A. Promoting Methane Hydrate Formation for Natural Gas Storage over Chabazite Zeolites. *ACS Appl. Mater. Interfaces* **2021**, *4* (12), 13420−13424.

(39) Kim, N. J.; Park, S. S.; Shin, S. W.; Hyun, J. H.; Chun, W. An experimental investigation into the effects of zeolites on the formation of methane hydrates. *Int. J. Energy Res.* **2015**, *39* (1), 26−32.

(40) Liu, H.; Zhan, S.; Guo, P.; Fan, S.; Zhang, S. Understanding the characteristic of methane hydrate equilibrium in materials and its potential application. *Chem. Eng. J.* **2018**, *349*, 775−781.

(41) Kang, S. P.; Lee, J. W. Formation characteristics of synthesized natural gas hydrates in meso- and macroporous silica gels. *J. Phys. Chem. B* **2010**, *114* (20), 6973−6978.

(42) Shi, B.-H.; Yang, L.; Fan, S.-S.; Lou, X. An investigation on repeated methane hydrates formation in porous hydrogel particles. *Fuel* **2017**, *194*, 395−405.

(43) Ling, Z.; Zhou, H.; Dong, H.; Shi, C.; Zhao, J.; Liu, H.; Song, Y. MXene (Ti3C2Tx) as a Promising Substrate for Methane Storage via Enhanced Gas Hydrate Formation. *J. Phys. Chem. Lett.* **2021**, *12* (28), 6622−6627.

(44) Wang, Z. Y.; Duan, J.; Chen, S. J.; Fu, Y.; Li, X. F.; Wang, D.; Zhang, M.; Zhang, Z. Q.; Liu, D. D.; Wang, F. H. A review on high-density methane storage in confined nanospace by adsorption-hydration hybrid technology. *J. Energy Storage* **2022**, *50*, No. 104195.

(45) Zhang, G.; Liu, Z.; Kong, Y.; Wang, F. Hydrate-based adsorption-hydration hybrid approach enhances methane storage in wet MIL-101(Cr)@AC under mild condition. *Chem. Eng. J.* **2023**, *472*, No. 145068.

(46) Zhang, X.-X.; Liu, H.; Sun, C.-Y.; Xiao, P.; Liu, B.; Yang, L.-Y.; Zhan, C.-H.; Wang, X.-Q.; Li, N.; Chen, G.-J. Effect of water content on separation of $CO_2/CH_4$ with active carbon by adsorption−hydration hybrid method. *Sep. Purif. Technol.* **2014**, *130*, 132−140.

(47) Fengyi, M.; Zhongjin, H.; Guosheng, J.; Fulong, N. Molecular insights into the effects of lignin on methane hydrate formation in clay nanopores. *Energy* **2023**, *276*, No. 127496.

(48) Hao, Y.; Xu, J.; Yuan, S.; Meng, Z.; Wang, X.; Xue, J.; Zhang, J. Molecular dynamics study of electric field enhanced hydrate growth for gas storage. *J. Nat. Gas Sci. Eng.* **2022**, *103*, No. 104617.

(49) He, Z.; Zhang, K.; Jiang, J. Formation of $CH_4$ Hydrate in a Mesoporous Metal-Organic Framework MIL-101: Mechanistic Insights from Microsecond Molecular Dynamics Simulations. *J. Phys. Chem. Lett.* **2019**, *10* (22), 7002−7008.

(50) He, Z. J.; Jiang, J. W.; Jiang, G. S.; Ning, F. L. Competition between $CH_4$ hydrate formation and phase separation in a wetted metal-organic framework MIL-101 at moderate subcooling: molecular insights into $CH_4$ storage. *J. Mater. Chem. A* **2024**, *12* (8), 4447−4459.

(51) Wang, Z.; Duan, J.; Chen, S.; Fu, Y.; Zhang, Y.; Wang, D.; Pei, J.; Liu, D. Molecular insights into hybrid $CH_4$ physisorption-hydrate growth in hydrophobic metal−organic framework ZIF-8: Implications for $CH_4$ storage. *Chem. Eng. J.* **2022**, *430*, No. 132901.

(52) Duan, J.; Jiang, X.; Fu, Y.; Chen, S.; Zi, M. Molecular insights into $CH_4/H_2O$ transport and hydrate formation in hydrophobic metal-organic frameworks ZIF-8: Implication for $CH_4$ storage by adsorption-hydration hybrid method. *Fuel* **2023**, *337*, No. 126851.

(53) Li, Z.; Li, N.; Kan, J. Y.; Liu, B.; Chen, G. J. Competitive and synergistic mechanisms of adsorption-hydration during methane storage in the wet ZIF-8 fixed bed. *Fuel* **2023**, *351*, No. 129055.

(54) Wu, Y.; He, Y.; Tang, T.; Zhai, M. Molecular dynamic simulations of methane hydrate formation between solid surfaces: Implications for methane storage. *Energy* **2023**, *262*, No. 125511.

(55) Lvov, Y. M.; Shchukin, D. G.; Mohwald, H.; Price, R. R. Halloysite clay nanotubes for controlled release of protective agents. *ACS Nano* **2008**, *2* (5), 814−820.

(56) Joussein, E.; Petit, S.; Churchman, J.; Theng, B.; Righi, D.; Delvaux, B. Halloysite clay minerals—A review. *Clay Miner.* **2005**, *40* (4), 383−426.

(57) Em, Y.; Stoporev, A.; Semenov, A.; Glotov, A.; Smirnova, E.; Villevald, G.; Vinokurov, V.; Manakov, A.; Lvov, Y. Methane Hydrate Formation in Halloysite Clay Nanotubes. *ACS Sustainable Chem. Eng.* **2020**, *8* (21), 7860−7868.

(58) Stoporev, A.; Mendgaziev, R.; Artemova, M.; Semenov, A.; Novikov, A.; Kiiamov, A.; Emelianov, D.; Rodionova, T.; Fakhrullin, R.; Shchukin, D. Ionic clathrate hydrates loaded into a cryogel— halloysite clay composite for cold storage. *Appl. Clay Sci.* **2020**, *191*, No. 105618.

(59) Mi, F. Y.; He, Z. J.; Fang, B.; Ning, F. L.; Jiang, G. S. Molecular insights into the effects of surface property and pore size of non-swelling clay on methane hydrate formation. *Fuel* **2022**, *311*, No. 122607.

(60) Ferrante, F.; Armata, N.; Lazzara, G. Modeling of the Halloysite Spiral Nanotube. *J. Phys. Chem. C* **2015**, *119* (29), 16700−16707.

(61) Jorgensen, W. L.; Madura, J. D.; Swenson, C. J. Optimized Intermolecular Potential Functions for Liquid Hydrocarbons. *J. Am. Chem. Soc.* **1984**, *106* (22), 6638−6646.

(62) Abascal, J. L. F.; Sanz, E.; Garcia Fernandez, R.; Vega, C. A potential model for the study of ices and amorphous water: TIP4P/Ice. *J. Chem. Phys.* **2005**, *122* (23), No. 234511.

(63) Cygan, R. T.; Liang, J. J.; Kalinichev, A. G. Molecular models of hydroxide, oxyhydroxide, and clay phases and the development of a general force field. *J. Phys. Chem. B* **2004**, *108* (4), 1255−1266.

(64) Mi, F. Y.; He, Z. J.; Cheng, L. W.; Jiang, G. S.; Ning, F. L. Molecular dynamics simulation on methane hydrate formation in clay nanopores of edge surfaces. *Appl. Clay Sci.* **2023**, *243*, No. 107069.

(65) Mi, F.; He, Z.; Jiang, G.; Ning, F. Effect of Glucose on $CH_4$ Hydrate Formation in Clay Nanopores and Bulk Solution: Insights from Microsecond Molecular Dynamics Simulations. *ACS Sustainable Chem. Eng.* **2024**, *12* (11), 4644−4654.

(66) Darden, T.; York, D.; Pedersen, L. Particle mesh Ewald: An N·log(N) method for Ewald sums in large systems. *J. Chem. Phys.* **1993**, *98* (12), 10089−10092.

(67) Mi, F.; He, Z.; Jiang, G.; Ning, F. Effects of marine environments on methane hydrate formation in clay nanopores: A molecular dynamics study. *Sci. Total Environ.* **2022**, *852*, No. 158454.

(68) Nosé, S. A Molecular-Dynamics Method for Simulations in the Canonical Ensemble. *Mol. Phys.* **1984**, *52* (2), 255−268.

(69) Parrinello, M.; Rahman, A. Crystal-Structure and Pair Potentials—A Molecular-Dynamics Study. *Phys. Rev. Lett.* **1980**, *45* (14), 1196−1199.

(70) Hess, B.; Kutzner, C.; van der Spoel, D.; Lindahl, E. GROMACS 4: Algorithms for Highly Efficient, Load-Balanced, and Scalable Molecular Simulation. *J. Chem. Theory Comput.* **2008**, *4* (3), 435−447.